DOPANT MAPPING FOR LASER DOPING USING SECONDARY ELECTRON IMAGE

Lujia Xu[1], Klaus Weber[1], Sieu Pheng Phang[1], Andreas Fell[1], Frank Brink[2], Evan Franklin[1]
[1]Centre for Sustainable Energy Systems, Australian National University, Canberra, ACT 0200, Australia
[2]Centre for Advanced Microscopy, Australian National University, Canberra, ACT 0200, Australia

ABSTRACT: In recent years, lasers have been widely used in fabrication processes for solar cells. One of the most promising applications of lasers in solar cell manufacturing is laser doping. Laser doping creates locally doped regions, such as those required to create selective emitters or locally doped rear-contact structures, via an industrially feasible manufacturing process. Mapping the dopant distribution of laser doped cross-sections is an effective way to rapidly qualify laser doping. However, the laser doping line width is only tens of microns, which makes characterization quite difficult. Until now, such investigation involves expensive and complex methods, for example SIMS and EBIC. This paper describes a novel cheap method with simple sample preparation to image cross-sectional dopant distribution of laser doped regions using dopant related contrast observed in secondary electron microscopy (SEM) images. To our knowledge, this is the first time that this method has been applied on delineating laser doping cross-sections. It is found that this technique can be used for different dopant sources and different doping methods under relatively wide FESEM work condition window. This method is proved to be a fast technique to investigate the influence of laser parameters on laser doping. In conjunction with alkaline etching, we also demonstrate that this method can effectively evaluate the risk of metallization shunt near the edges of dielectric film windows opened by laser.
Keywords: SEM, laser doping

1 INTRODUCTION

An effective way to evaluate the quality of laser doping is to measure its cross-sectional dopant distribution. Previous researchers have achieved this goal using Secondary Ion Mass Spectroscopy (SIMS)[1-9] and Electron Beam Induced Current (EBIC)[5]. SIMS is the most widely used method to measure laser doping depth profile**.**It involves sputtering the sample and mass analyzing the atoms that come off [10]. SIMS has high sensitivity to dopant concentration, but there are also two obvious disadvantages. Firstly, SIMS cannot distinguish between active and inactive dopants [10]. Secondly, the spatial resolution of SIMS is limited, so that the depth profile values obtained from SIMS are mean values over a relative large area[1],[5]. The main drawback of the EBIC technique is that the shape of the EBIC curve depends on the surface recombination velocity of the surface where the beam impinges[11]. Except these theoretical disadvantages, SIMS and EBIC are both time-consuming and expensive. In addition, not all researchers can easily find a nearby organization who offers SIMS or EBIC. Therefore, identifying fast and cheap dopant mapping methods is of great interest. In this paper, Secondary electron microscopy dopant contrast image (SEMDCI), will be applied in order to image laser doped cross-sections. To the author's knowledge, this is the first time the technique has been applied for this purpose. We demonstrate that it is an effective, fast and cheap characterization method for laser doping work.

It was first observed in 1967 that a contrast exists between p-doped and n-doped regions in secondary electron (SE) images in the scanning electron microscope (SEM), where p-doped regions appear brighter than n-doped regions[12]. However, due to the equipment limitations, this technique was not widely used in the following decades. With the development of field emission gun SEMs (FESEM), the topic was revived in 1995. Perovic et al. found the contrast observed by SEM images is not only related to doping type but also depends on doping concentration levels, and observed a linear relationship between the observed contrast and the logarithm of the dopant concentration in p-type Si[13]. Following reports from different researchers confirmed this finding for dopant concentrations in the range of 10^{16} –10^{20} cm^{-3}.[13-16]. The most significant advantage of SEMDCI is its fast data measurement speed, high spatial sensitivity (as thin as 1 nm doped line was detected [14]) and simple sample preparation.

In this paper, we will show the impact of different laser powers and laser scan speeds on the dopant distributions of laser doping cross-sections using SEMDCI technique. This characterization method will also be used to delineate laser doping regions near the edge of dielectric film windows, which is important for investigating possible metallization shunts near the edges of laser doped regions.

2 SAMPLE PREPARATION

100mm n-type Cz <100> single sided polished 525±25μm thick and 1-20 Ω.cm wafers were used for laser doping sample. For some specific experiments, SiO_2 was deposited on wafers surface. Texture etched wafers were prepared for both boron and phosphorus diffusion. The dopant source for laser doping is boron-spin-on dopant (B-SOD). Laser doped lines were created using a DPSS 532nm laser source with different laser powers, laser scan speeds and scan passes, using Q-switch mode at 100kHz. Samples were immediately cleaved just before loading into FESEM. The FESEM equipment used here is a Zeiss UltraPlus FESEM located in Centre for Advanced Microscopy (CAM) at the ANU.

3 SEMDCI PARAMETERS

Four main FESEM parameters are considered here: detector type, accelerating voltage (AV), working distance (WD) and aperture size. To isolate the influence of each parameter, when one parameter was taken as variable, all other parameters were kept constant.

Back scatter electron (BSE) that is directly related to changes in the mean atomic number is not considered capable of imaging the dopant contrast of semiconductors [14],[16-18]. Therefore, only secondary electron

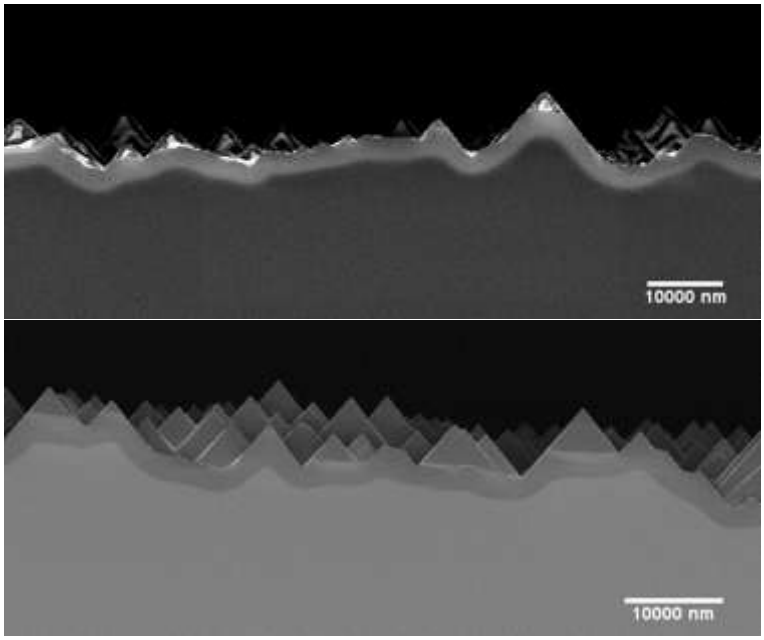

(a)

(b)

Figure 1 Application of SEMDCI to the delineation of diffused surface regions of texture surfaces: (a) boron diffusion on n type textured substrate (b) phosphorus diffusion on p type textured substrate

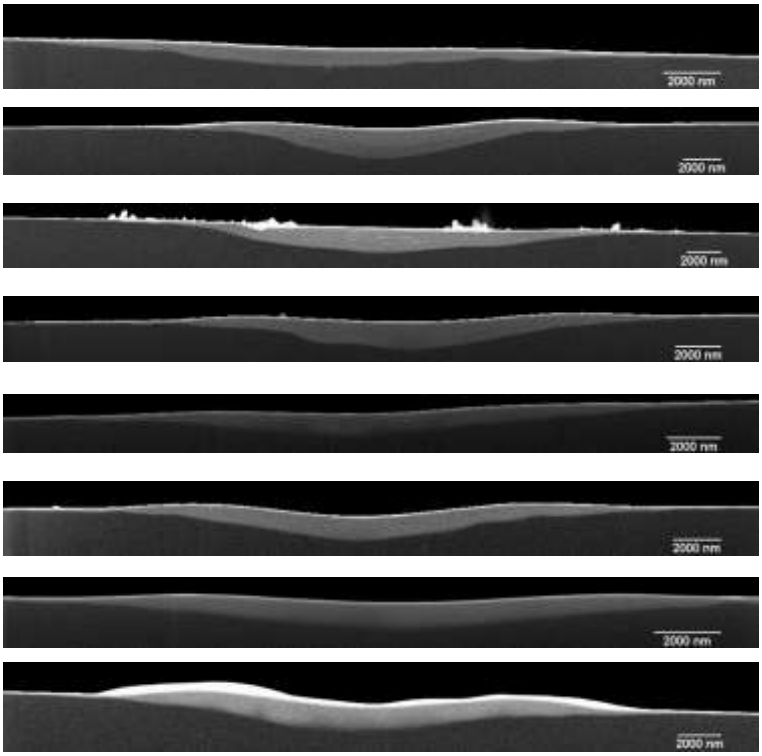

(a)

(b)

(c)

(d)

(e)

(f)

(g)

(h)

Figure 2 The influence of different laser parameters (at 100kHz Q-switch mode) on laser doping cross-section characterized by SEMDCI: (a) 1.24W 20mm/s (b)1.64W 10mm/s (c)1.64W 10 mm/s 5passes (d) 1.64W 20mm/s (e) 1.64W 100mm/s (f) 1.64W 100mm/s 5passes (g) 1.64W 50mm/s 5passes (h) 2.22W 500mm/s 5passes

detectors were used in experiments. Theoretically, the dopant contract could be seen in both the upper (through-the-lens) and lower (conventional SEs) detectors, but the contrast is enhanced by through-the-lens mode [16],[17],[19]. Practically, the dopant contrast was seldom observed in conventional SEs mode, but only in through-the-lens mode.

Accelerating voltage (AV) from 0.5 to 20kV was used in previous literature [14],[16],[18-21] for dopant contrast delineation. In our experiments, for p type laser doping samples, the dopant contrast will vanish when the accelerating voltage is higher than 7kV. Considering the doping concentration of laser doping samples are more uniform and mostly higher than diffusion samples, the reason why under high AV, for p type sample, diffusion sample reported in literature can be seen but laser doping sample cannot is unknown yet. Though the accelerating voltage working window is relatively wide, too low or

too high accelerating voltage should be avoid. Low accelerating voltage is likely to cause sample surface contamination, high image noise and difficult in focus finding, while high accelerating voltage tend to result in electron scan damage and significantly edge effect

Relatively short WD (below 6mm) were used by previous researchers [14],[16],[20],[22],[23]. It was reported that shorter WD will enhance the dopant contrast in most case [16],[22]. However, Schonjahn *et al* found opposite phenomenon. They found that detector's collection angle is a function of the WD and decreases for larger WD. Considering the dopant contrast is also related to SEs angular distribution, the contrast for a small WD was found always lower than for a large WD in their experiments[24]. Practically, in this work, it is found for p- type laser doping, dopant contrast can be seen at WD from 1-6mm. Though dopant contrast can still be seen at WD as large as 10mm for some samples, large WD will significantly increase the image noise and reduce the image resolution. Low WD, such as 1 mm, is not suggested because of obvious electron scan damage.

Using different aperture sizes under the same AV is actually an indirect way to adjust beam current. It is found that small apertures will significantly reduce the signal intensity, while large apertures result in low resolution, significant substrate charging and a strong edge effect. Medium apertures were found to be optimal and were used in this work.

An example of the good contrast that can be obtained by the appropriate choice of FESEM (as well as substrate doping) parameters is shown in Figure 1 and also a good example that the application of SEMDCI on solar cell is not only limited to laser doping is the ability to display the diffusion regions of surface-textured samples.

4 LASER PARAMETERS INFLUENCE

The results of SEMDCI for laser doping are shown in Figure 2. From the images, the impact of different laser parameters on cross-sectional dopant distribution can be clearly seen. Comparing Figure 2 (a) and (d), we find that under the same laser scan speed and number of passes, higher energy results in deeper doping as well as a more uneven surface. As for same laser power and same scan speed but different number of passes (e.g. Figure 2 (b) and (c); (e) and (f)), the results differs for different scan speeds: for low scan speed, multiple passes did not change the doped depth significantly, but resulted in a smoother surface; for high scan speed, multiple passes performs similar as increasing laser power as in Figure 2 (a) and (d). As to same laser power, same number of passes but different scan speeds (e.g. Figure 2 (b) (d) and (e)), lower scan speed also works similar as increasing laser power as in Figure 2 (a) and (d). From Figure 2 (h), we can see high laser power combined with high scan speed and multiple passes is a way to avoid ablation at high laser power and to achieve wanted depth laser doped region with less process time. However attention has to be paid to the surface condition and dopant distribution continuity in this situation.

5 LASER DOPING REGIONS NEAR THE EDGE OF DIELECTRIC FILM WINDOWS

From Figure 2, we can see that the laser doped line widths measured according to the edges of the contrast patterns are in the order of 20 to 30μm. However, this width is not necessarily the dimension of the dielectric film windows. In normal laser doping processes, the laser will open windows in the dielectric films which serve as both emitter passivation layers and metallization mask. Special attention needs to be paid to the doped region near the edge of dielectric film windows, since if the depth of the junction here is too shallow, during following metallization procedure, metal may penetrate the doped region and directly contact the substrate, resulting in a shunt. It would be desirable if the laser doped regions can laterally extend into the parts

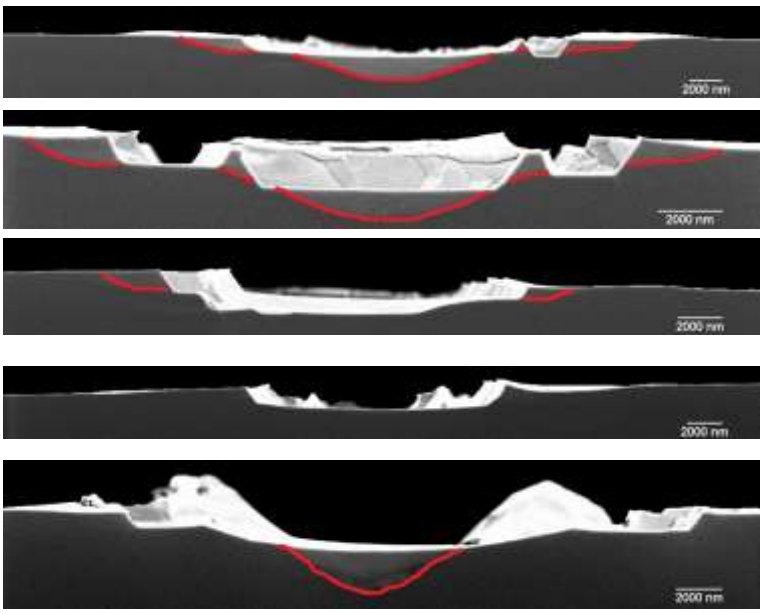

Figure 3 The depth of laser doping regions at the edge of dielectric film windows with different laser parameters (at 40 kHz Q-switch mode): (a) 0.66W 4mm/s 5 passes (b)0.66W 4mm/s (c)0.66W 8mm/s (d)0.66W 40mm/s 5passes (e) 0.89W 200mm/s 5passes. For reader's convenience, the contrast boundaries were indicated with red lines

underneath the dielectric films and have a reasonable depth near the window edges. SEMDCI offers a promising method to detect this edge covering effect.
90 nm SiO2 film was grown on surface before applying B-SOD and laser process. After laser process, samples were etched in tetramethylammonium hydroxide (TMAH) for 1 min. In this case, only those parts of the silicon exposed to the etching solution were selectively etched, but not these parts protected by the SiO_2 films. After TMAH etching, residual dielectric films were removed by HF dipping in order to avoid charge effects in the FESEM. Results are displayed in Figure 3. From the SEMDCI, we can easily see, under some laser parameters, laser doped regions laterally extend under the SiO2 film and have relatively deep junctions near the edges of dielectric film (See Figure 3 (a) (b) and (c)). In contrast, high scan speeds result in less lateral extension and shallow junctions near edges, meaning increased risk of metallization shunt, e.g. Figure 3 (d). One thing worth mentioning here is that the combination of high laser power and fast scan speed achieves deep depth in the center of doped region but does not offer good quality near the edge dielectric films.

6 CONCLUSION

The SEMDCI offer a fast, cheap and simple method to characterize the quality of laser doping. From SEMDCI, important information, such as p-n junction depth, junction outline, junction lateral extension, surface bump degree and *etc.*, can be clearly delineated. This information enables researchers to evaluate the property of laser doping and the influence of sample and laser parameters on laser doping results.

7 ACKNOWLEDGE

The authors thank Di Yan, Fiacre Rougieux and Hua Chen (ANU, Australia) for helpful discussion and the help on FESEM operation.

8 REFERENCE

[1] A. Fell, D. Kray, T. Wütherich, R. Müller, G. P. Willeke, and S. W. Glunz, presented at the 23rd European Photovoltaic Solar Energy Conference, Valencia, Spain, 2008.

[2] S. Hopman, A. Fell, K. Mayer, M. Aleman, M. Mesec, R. Mueller, D. Kray, and G. P. Willeke, presented at the 22th European Photovoltaic Solar Energy Conference, Milan, Italy, 2007.

[3] T. C. Röder, S. J. Eisele, P. Grabitz, C. Wagner, G. Kulushich, J. R. Köhler, and J. H. Werner, *Progress in Photovoltaics: Research and Applications*, vol. 18, pp. 505-510, 2010.

[4] D. K. Schroder, *Semiconductor material and device characterization* Wiley-IEEE Press, 2006.

[5] Z. Hameiri, L. Mai, T. Puzzer, and S. R. Wenham, *Solar Energy Materials and Solar Cells*, vol. 95, pp. 1085-1094, 2011.

[6] G. Poulain, C. Boulord, D. Blanc, A. Kaminski, M. Gauthier, C. Dubois, B. Semmache, and M. Lemiti, *Applied Surface Science*, vol. 257, pp. 5241-5244, 2011.

[7] M. Okanovic, U. Jaeger, M. Ahrens, U. Stute, A. Grohe, and R. Preu, presented at the 24th European Photovoltaic Solar Energy Conference,, Hamburg, Germany, 2009.

[8] B. Paviet-Salomon, S. Gall, R. Monna, S. Manuel, and A. Slaoui, *Solar Energy Materials and Solar Cells*, vol. 95, pp. 2536-2539, 2011.

[9] Z. Hameiri, T. Puzzer, L. Mai, A. B. Sproul, and S. R. Wenham, *Progress in Photovoltaics: Research and Applications*, vol. 19, pp. 391-405, 2011.

[10] M. R. Castell, D. A. Muller, and P. M. Voyles, *Nature Materials*, vol. 2, pp. 129-144, 2003.

[11] T. Meoded, R. Shikler, N. Fried, and Y. Rosenwaks, *Applied Physics Letters*, vol. 75, pp. 2435-2437, 1999.

[12] T. H. P. Chang and W. C. Nixon, *Solid State Electronics*, vol. 10, pp. 701-702,IN9-IN10,703-704, 1967.

[13] D. D. Perovic, M. R. Castell, A. Howie, C. Lavoie, T. Tiedje, and J. S. W. Cole, *Ultramicroscopy*, vol. 58, pp. 104-113, 1995.

[14] S. L. Elliott, R. F. Broom, and C. J. Humphreys, *Journal of Applied Physics*, vol. 91, pp. 9116-9122, 2002.

[15] D. Venables, H. Jain, and D. C. Collins, *Journal of Vacuum Science and Technology B: Microelectronics and Nanometer Structures*, vol. 16, pp. 362-366, 1998.

[16] C. P. Sealy, M. R. Castell, and P. R. Wilshaw, *Journal of Electron Microscopy*, vol. 49, pp. 311-321, 2000.

[17] D. C. Joy and C. S. Joy, *Micron*, vol. 27, pp. 247-263, 1996.

[18] I. Müllerová, M. M. El-Gomati, and L. Frank, *Ultramicroscopy*, vol. 93, pp. 223-243, 2002.

[19] D. Venables and D. M. Maher, *Journal of Vacuum Science & Technology B: Microelectronics and Nanometer Structures*, vol. 14, pp. 421-425, 1996.

[20] C. Schönjahn, C. J. Humphreys, and M. Glick, *Journal of Applied Physics*, vol. 92, pp. 7667-7671, 2002.

[21] M. El-Gomati, F. Zaggout, H. Jayacody, S. Tear, and K. Wilson, *Surface and Interface Analysis*, vol. 37, pp. 901-911, 2005.

[22] I. Volotsenko, M. Molotskii, Z. Barkay, J. Marczewski, P. Grabiec, B. Jaroszewicz, G. Meshulam, E. Grunbaum, and Y. Rosenwaks, *Journal of Applied Physics*, vol. 107, pp. 014510-7, 2010.

[23] P. Kazemian, C. Rodenburg, and C. J. Humphreys, *Microelectronic Engineering*, vol. 73-74, pp. 948-953, 2004.

[24] C. Schönjahn, R. F. Broom, C. J. Humphreys, A. Howie, and S. A. M. Mentink, *Applied Physics Letters*, vol. 83, pp. 293-295, Jul 2003.